A Global–Local Approach for Mechanical Deformation and Fatigue Durability of Microelectronic Packaging Systems

T. Zhang

S. Rahman
Professor
e-mail: rahman@engineering.uiowa.edu

K. K. Choi

Department of Mechanical & Industrial Engineering,
The University of Iowa,
Iowa City, IA 52242

K. Cho

P. Baker

M. Shakil

D. Heitkamp

Rockwell Collins, Inc.,
Cedar Rapids, IA 52498

This paper presents a global–local methodology for predicting mechanical deformation and fatigue durability of solder joints in electronic packaging systems subject to cyclic thermal loading. It involves a global deformation analysis, a local critical solder–joint analysis, and a fatigue life analysis. The global deformation analysis includes a new optimization formulation for determining an equivalent model. The methodology developed was applied to fine pitch ball grid array (fpBGA) and super ball grid array (SBGA) packages. Selective experimental efforts were also undertaken to evaluate the predicted deformation characteristics of the fpBGA package. A good agreement was obtained between the simulated deformation results and experimental observations. For the durability analysis, the total fatigue life predicted using the energy-based method is larger than 2500 cycles—a trend observed experimentally for both packages entailing widely different designs. Based on proposed modeling and simulation results and package designs studied, the SBGA package is more durable than the fpBGA package.
[DOI: 10.1115/1.2721092]

Keywords: global-local, equivalent model, submodel, fatigue crack initiation, HASMAP, Moiré interferometry

1 Introduction

Commercial-off-the-shelf (COTS) electronics are being utilized on military and commercial platforms to leverage technology growth and maximize affordability. The traditional approach to the selection and evaluation of COTS and emerging packaging technologies is heavily reliant on accelerated durability testing. Such testing is costly and protracted and often requires revalidation when changes occur in the design or manufacturing processes. In addition, currently there are no substantiated and meaningful extrapolations of the accelerated test data to longer-term operational environments. Modeling and simulation are therefore necessary for rapid assessment of fatigue durability of commercial packaging before their induction into products. However, such methodologies need to be based on the physics-of-failure models duly backed up by rigorous experimental validation.

The low-cycle fatigue is a common failure mechanism in solder joints in the electronic packaging industry. The cyclic thermal loading combined with the mismatch in thermal expansion properties for various components of the assembly lead to stress reversals and accumulation of inelastic strain in solder joints. Since the solder material exhibits creep deformation characteristics, a nonlinear viscoelastic or viscoplastic finite element analysis (FEA) is often needed to calculate the fatigue life. Such a detailed analysis can become computationally demanding and even prohibitive. To overcome this problem, there has been a recent surge in global–local approaches [1–5], mostly in conjunction with FEA, which involve a global analysis for predicting displacement field around a critical solder joint; a local analysis for predicting stress and strain fields of that critical joint; and a fatigue life analysis using phenomenological equations. While these global–local approaches significantly reduce the computational effort, there are several shortcomings. First, the equivalent beams or equivalent solids employed for the simplified representation of solder geometry in existing global models is based on volume equivalence or alternative equivalence criteria [1–3]. Depending on the type of package design and its response characteristics, an equivalent global model based on volume equivalence alone may provide grossly inaccurate results. Second, many fatigue life predictions in existing global–local approaches are based on phenomenological equations, which are derived from testing either small-scale solder specimens [6–11] or like-design packages [12]. Unfortunately, these phenomenological equations are of a highly empirical nature, are solely applicable to fatigue crack initiation, and cannot account for crack propagation, which may be a significant part of the total life of a solder joint [7,8]. Third, the current packaging literature is replete with numerous simulation-based methodologies, but their predictive capability can be limited unless there is meaningful correlation with experimental observation entailing wide ranges of the package design, materials, and environments.

This paper presents a simulation methodology in the spirit of the global–local approach for predicting mechanical deformation and fatigue durability of solder joints in electronic packaging systems subject to cyclic thermal loading. Section 2 describes the methodology, which involves a global deformation analysis, a local critical solder–joint analysis, and a fatigue life analysis. The methodology developed has been applied to fine-pitch ball-grid array (fpBGA) and super BGA (SBGA) packages, the geometric details, material properties, and thermal loads of which are presented in Sec. 3. The equivalent global model, selective experimental validation of the deformation, and fatigue life analysis are reported in Secs. 4–6. Finally, Sec. 7 provides summary and conclusion from this work.

Contributed by the Electrical and Electronic Packaging Division of ASME for publication in the JOURNAL OF ELECTRONIC PACKAGING. Manuscript received February 9, 2006; final manuscript received July 5, 2006. Review conducted by Bongtae Hun.

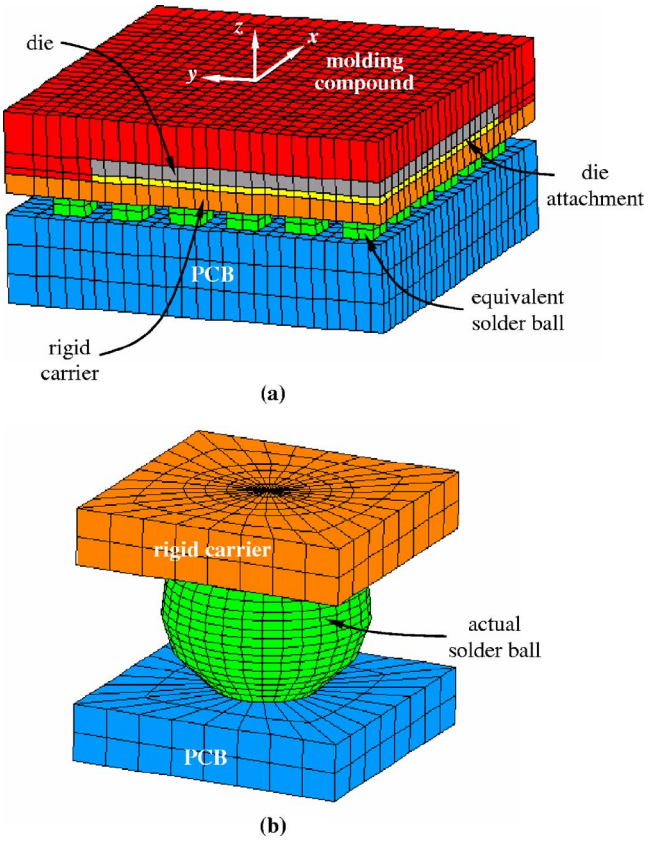

Fig. 1 A schematic of the global–local methodology: (*a*) global model; and (*b*) local model

2 A Proposed Global–Local Methodology

A global–local methodology for predicting mechanical deformation and fatigue durability of solder joints under cyclic thermal loads has been examined by The University of Iowa and Rockwell Collins, Inc. team. It involves three major steps: (1) a global deformation analysis employing an optimal geometry of equivalent solder joints derived from nonlinear load–deformation response; (2) a local critical solder–joint analysis involving rigorous application of nonlinear submodeling technique; and (3) a fatigue life analysis including fatigue crack initiation and crack-propagation. Figure 1 shows a schematic representation of the global–local methodology.

2.1 Global Deformation Analysis. The objectives of the global analysis are to identify a critical solder joint in an assembly and to calculate displacement fields surrounding a critical solder joint. The analysis entails a coarse three-dimensional FEA model involving 8- or 20-noded solid elements for all components of the package assembly including equivalent solder joints; linear–elastic material constitutive law for various package components (rigid carrier, die chip, die attachment, molding compound, etc.) and printed circuit board (PCB); and viscoelastic or viscoplastic constitutive law for the solder material. Although the coarseness of the global model is intended for computational efficiency, the accuracy of the resulting displacement solution must be adequate and acceptable. Hence, equivalent models for solder joints must be carefully selected for generating accurate displacement fields. A new equivalence criterion is proposed, as follows.

There are several options for selecting the shape of an equivalent solder joint, such as the brick shape (one-parameter model), the diamond shape (two-parameter model), and a general shape (n-parameter model), as shown in Fig. 2. The library of these competing options can be further expanded by accommodating more general and complex shapes. Nevertheless, given a shape of an equivalent model, its parameters must be evaluated using nonlinear response characteristics from the actual solder–joint geometry and equivalence criteria. The optimization algorithm developed to obtain an equivalent model involves four steps: (1) select an equivalent model with an n-dimensional width vector $\boldsymbol{w} = \{w_1, \ldots, w_n\}^T$, where w_i is the ith width parameter, from the library of competing models; (2) create a global FEA model by replacing all solder joints with the equivalent model from Step 1 and conduct nonlinear FEA of the package–board assembly subject to prescribed thermal cycles. Average the displacements over all nodes at the top ($\boldsymbol{u}_t(\boldsymbol{w};t)$) and bottom ($\boldsymbol{u}_b(\boldsymbol{w};t)$) surfaces separately of the critical solder joint with the equivalent shape and denote their difference by the relative displacement history $\Delta\boldsymbol{u}(\boldsymbol{w};t) \equiv \boldsymbol{u}_t(\boldsymbol{w};t) - \boldsymbol{u}_b(\boldsymbol{w};t)$, where t is the time; (3) Perform two separate nonlinear FEA, one for a coarsely discretized equivalent model of the solder joint fixed at the bottom and the other for a finely discretized actual geometry of the solder joint also fixed at the bottom, both subjected to the relative displacement history $\Delta\boldsymbol{u}(\boldsymbol{w};t)$ from Step 2 and applied at the top surface. Let $R_e(\Delta\boldsymbol{u}(\boldsymbol{w},t);\boldsymbol{w})$ and $R_a(\Delta\boldsymbol{u}(\boldsymbol{w},t))$ denote two time histories of total reaction forces at bottom surfaces of the equivalent model and the actual solder joint, respectively; and (4) If $\epsilon_1(t;\boldsymbol{w})$

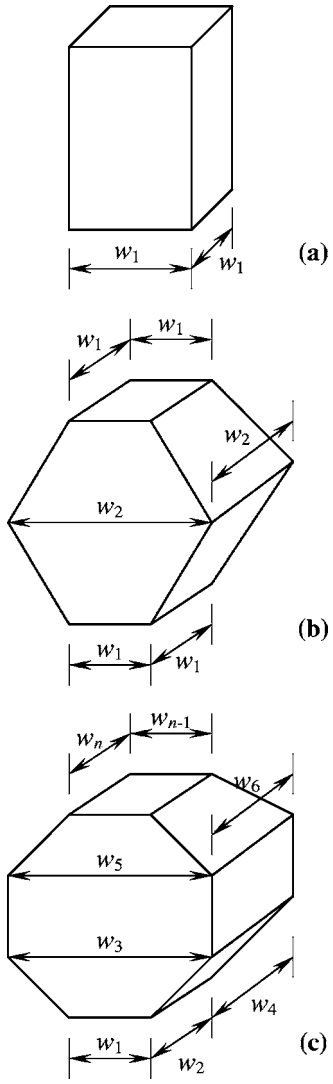

Fig. 2 Various possible shapes of equivalent model for solder joint: (*a*) brick; (*b*) diamond; (*c*) general (e.g., eight-parameter model)

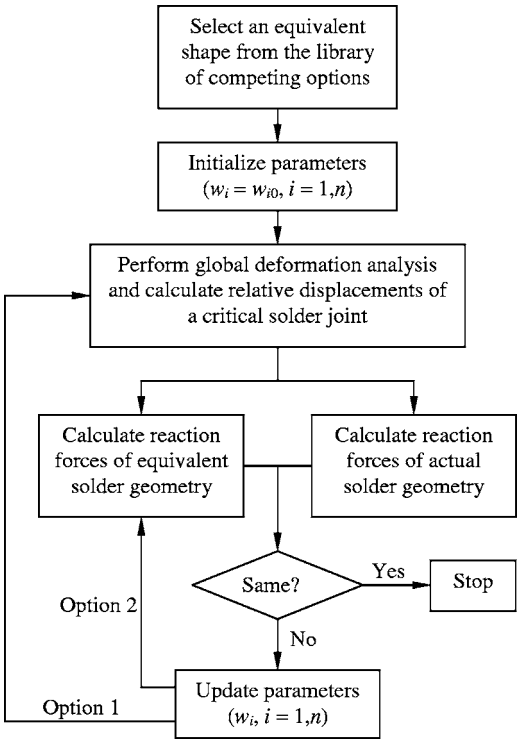

Fig. 3 Flowchart for calculating equivalent model parameters

$\equiv [R_e(\Delta \boldsymbol{u}(\boldsymbol{w},t);\boldsymbol{w}) - R_a(\Delta \boldsymbol{u}(\boldsymbol{w},t))]^2$ represents a difference between reaction forces from the equivalent model and the actual solder joint, optimal values of model parameters $w_1, \ldots, w_n$ can be determined by solving the constrained optimization problem

$$\min_{w} \quad \int \epsilon_1(t;\boldsymbol{w})dt \qquad \text{subject to} \quad l_i(\boldsymbol{w}) > 0, \quad i = 1, \ldots, n_c \tag{1}$$

where $l_i(\boldsymbol{w}), i = 1, \ldots, n_c$ are linear constraints related to the shape or size of the equivalent model and n_c is the total number of constraints. Option 1 of the flowchart in Fig. 3 describes the iteration procedure in solving the optimization problem in Eq. (1). However, Option 1 is expensive, because for every change of $\boldsymbol{w}$, additional global FEA have to be performed to generate $\Delta \boldsymbol{u}(\boldsymbol{w};t)$. An efficient alternative is to define a simplified optimization problem

$$\min_{w} \quad \int \epsilon_2(t;\boldsymbol{w})dt \qquad \text{subject to} \quad l_i(\boldsymbol{w}) > 0, \quad i = 1, \ldots, n_c \tag{2}$$

where $\epsilon_2(t;\boldsymbol{w}) \equiv [R_e(\Delta \boldsymbol{u}(\boldsymbol{w}_0,t);\boldsymbol{w}) - R_a(\Delta \boldsymbol{u}(\boldsymbol{w}_0,t))]^2$ and $\boldsymbol{w}_0$ is the initial value. Option 2 in Fig. 3 describes the iteration procedure in solving Eq. (2). Option 2 sidesteps additional global FEA when $\boldsymbol{w}$ changes, because the displacement time history $\Delta \boldsymbol{u}(\boldsymbol{w}_0;t)$ is obtained from the initial value. Therefore, Option 2 is easier to solve and is significantly less expensive than Option 1. Option 2 can be enhanced by an adaptive scheme, for example, by repeated application of Option 2, which involves employing a solution from an intermediate application as an initial guess for the following application. The authors' experience suggests that 1–3 iterations of Option 2 typically lead to a desired solution. A newly developed hybrid method entailing the response surface approximation and the pattern search algorithm was employed to solve the proposed optimization problem [13].

2.2 Local Critical Solder–Joint Analysis. A local FEA model involves constructing a detailed mesh of a critical solder joint (Fig. 1(*b*)) to accurately predict its stress, strain, strain energy density, and any response quantities of interest for the following durability analysis. The boundary conditions are derived from a nonlinear submodeling technique, also known as the cut-boundary displacement method. The cut boundary, which constitutes a boundary of the local model, represents a cut through the global model. Displacements calculated on the cut boundary of the global model are transferred as boundary conditions of the local model. However, cut boundaries should be located far enough away from regions of stress concentrations, such as the top and bottom surface of a critical solder joint. Accordingly, a critical solder joint, substrate, and PCB are included in the local model, as shown in Fig. 1(*b*). There is frequent confusion about the applicability of submodeling to nonlinear path-dependent problems. The question arises due to linear ramping of external loads in some FEA software tools [5], which may lead to erroneous submodeling results. For path-dependent problems, the load history is important and must be strictly followed to generate the time history of cut-boundary displacements for the local model.

The local analysis involves a fine-scale three-dimensional FEA model including 8- or 20-noded solid elements for the solder joint, substrate, and PCB; linear–elastic constitutive law for the substrate and PCB (see Fig. 1(*b*)); and viscoelastic or viscoplastic constitutive law for the solder. The same temperature history used in the global analysis is again applied to perform the local analysis.

2.3 Fatigue Life Analysis. Fatigue damage is usually the result of stress concentrations caused by dislocation pileups due to the inelastic slip motion of lattice defects and sliding between grains at the boundaries. Under cyclic thermal loads, there is a migration of dislocations that results in localized plastic deformation. Microscopic cracks are created that grow and coalesce to produce macroscopic cracks. The thermal fatigue of a solder joint is essentially a low-cycle fatigue phenomenon and depends not only on the cyclic temperature range, but also on the mean temperature, dwell times and temperatures, loading and unloading rates, solder microstructure, presence of intermetallic, alloying and trace elements, joint geometry and defects, and residual strains due to processing. Clearly, accounting in a rigorous way for all of these parameters is a formidable task. Nevertheless, crack initiation and crack propagation are commonly regarded as two major causes and phases of fatigue damage accumulation, leading to ultimate failure.

2.3.1 Fatigue Crack Initiation. A common approach for predicting fatigue crack-initiation life N_{is} is based on the strain-based Coffin–Manson equation [14]

$$\frac{\Delta \epsilon}{2} = \frac{\sigma_f' - \sigma_m}{E}(2N_{\text{is}})^b + \epsilon_f'(2N_{\text{is}})^c \tag{3}$$

where $\Delta\epsilon/2$ is the von Mises equivalent strain amplitude and σ_m is the mean stress, both of which are obtained from the local model; and E, σ_f', b, ϵ_f', and c are known material parameters representing elastic modulus, fatigue strength coefficient, fatigue strength exponent, fatigue ductility coefficient, and fatigue ductility exponent, respectively.

Recently, an energy-based approach [8] has become popular, in which crack initiation is identified on the basis of the critical strain energy during cyclic thermo-mechanical loading. Quite often the elastic energy is ignored by assuming that crack initiation is primarily dependent on the dissipated energy due to irreversible (inelastic) deformations. The fatigue crack-initiation life N_{ie} based on the energy approach is defined as

$$N_{\text{ie}} = K_1(\Delta W)^{K_2} \tag{4}$$

where ΔW is the cyclic inelastic (creep) strain energy density, which is obtained from the local model; and K_1 and K_2 are con-

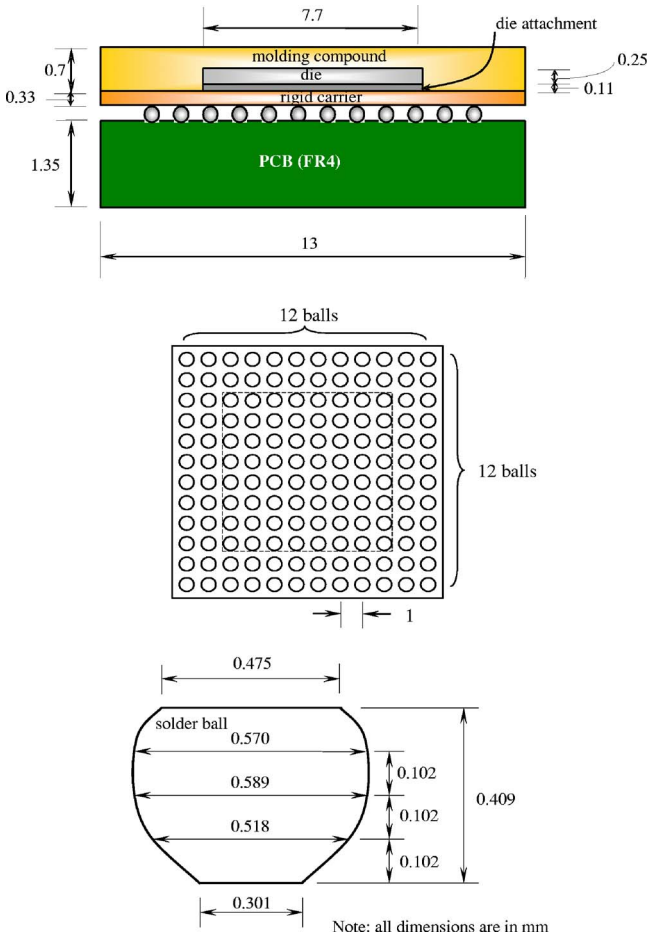

Fig. 4 The fpBGA package (all dimensions are in mm)

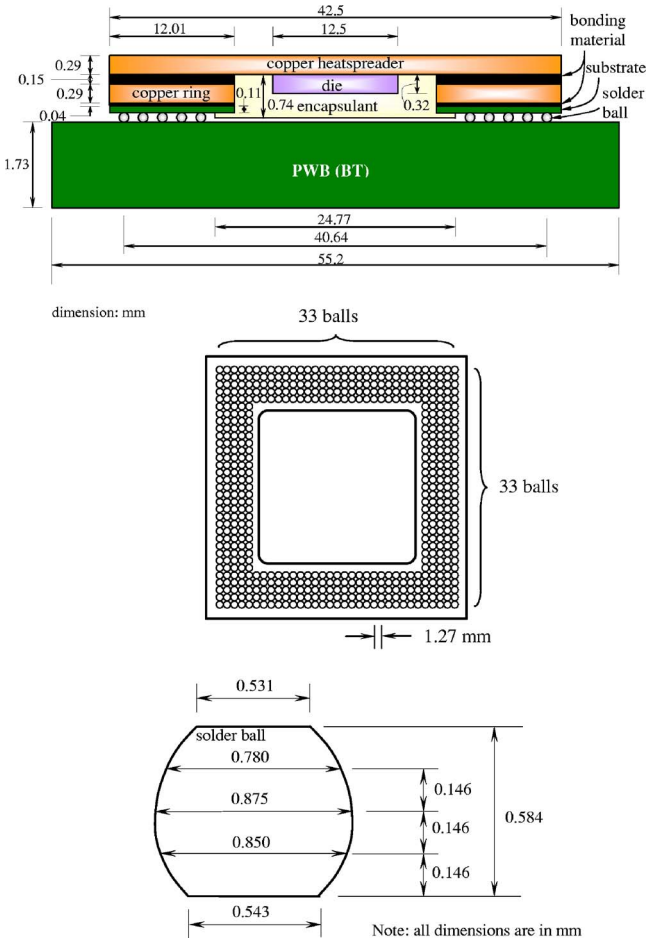

Fig. 5 The SBGA package (all dimensions are in mm)

stants calibrated from laboratory tests. Both Eqs. (3) and (4) are empirical equations for predicting the crack-initiation life.

2.3.2 Fatigue Crack Propagation. The damage accumulation concept involving inelastic strain energy density and fracture-mechanics parameters (e.g., *J*-integral, stress-intensity factors) can be used to predict crack growth under cyclic loads. Mathematical functions for crack propagation rate as proposed in various references have a generic form

$$\frac{da}{dN} = \varphi_1(a, D, \Delta D, R) \tag{5}$$

where a is the crack size at N cycles; φ_1 is a non-negative function; D is inelastic strain energy or fracture-mechanics parameter characterizing crack-driving force; ΔD is the range of the damage parameter; and R is the stress ratio. For example, starting from a known initial crack size, the remaining crack-propagation life N_p can be determined by integrating the crack-growth law [8]

$$\frac{da}{dN} = K_3(\Delta W)^{K_4} \tag{6}$$

where K_3 and K_4 are parameters of crack-growth kinetics typically estimated from small-scale laboratory specimens. In general, ΔW depends on the instantaneous crack length and is computationally expensive to evaluate, because ΔW must be obtained for each increment of the crack growth. A simplified and common assumption, which entails constant ΔW [8], may be employed to yield an explicit expression of the crack-propagation life

$$N_{\text{pe}} = \frac{a_c - a_0}{K_3(\Delta W)^{K_4}} \tag{7}$$

where a_0 and a_c are initial and final (critical) crack lengths, respectively. Equations (6) and (7) have been adopted by several researchers for solder joint applications [15–17]. Finally, by adding N_{ie} and N_{pe}, the total fatigue life $N = N_{\text{ie}} + N_{\text{pe}}$ of a solder joint can be predicted.

It is worth noting that a similar crack-propagation analysis involving the cracked area as a damage parameter may also be employed [18]. However, the associated crack-growth law and its parameters must be determined from relevant experimental data. They are subjects of future research.

3 Case Studies

Two BGA packages, fpBGA (144-I/O full array) and SBGA (560-I/O perimeter array), were studied to evaluate their deformation characteristics and crack-initiation lives using the proposed global–local methodology. Figures 4 and 5 define the package geometry of fpBGA and SBGA, respectively. The time-independent elastic material properties of package components and solder are defined in Tables 1 and 2, respectively [19]. The PCBs for fpBGA and SBGA are, respectively, made of FR4 and BT materials with their time-dependent elastic material properties defined in Tables 3 and 4 [19]. The thermal load profile for both packages involves temperature cycles varying from −55°C to 125°C and is defined in Fig. 6 [19]. Table 5 presents the parameters of the thermal loads for both packages.

The solder material is eutectic 63Sn–37Pb, which obeys the Garofalo–Arrhenius creep constitutive law [19]

Table 1 Elastic properties of fpBGA package components and solder

Material	Young's modulus (E) (Gpa)	Poisson's ratio (ν)	Coeff. of thermal exp. (α) (/°C)
Solder	24.83	0.4	21×10^{-6}
Rigid carrier	26	0.39	13×10^{-6}
Die attachment	16	0.25	14×10^{-6}
Die chip	131	0.3	4.1×10^{-6}
Molding compound	16	0.25	14×10^{-6}

$$\dot{\epsilon} = A(\sinh B\sigma)^n d^m \exp\left(-\frac{Q}{RT}\right) \tag{8}$$

where $\dot{\epsilon}$ is the creep strain rate; σ is the equivalent stress in MPa; T is the absolute temperature in Kelvin, constant $A=2.9524\times10^8$, grain size $d=5.5\ \mu$m, activation energy $Q=61.417$ J/k-mole, gas constant $R=8.314$ J/k mole, constant $B=0.125938$, stress exponent $n=1.88882$, and grain size exponent $m=3.011$. The parameters of Coffin–Manson equation employed for fatigue crack-initiation life of eutectic 63Sn–37Pb solder material are: $E=24.83$ MPa, $\sigma_f'=0.397$, $\epsilon_f'=0.396$, $b=-0.115$, and $c=-0.6$ [19]. The parameters of energy-based fatigue crack-initiation and crack-propagation lives are: $K_1=84{,}200$ cycles/psi^{K_2}, $K_2=-1.61$, $K_3=1.08\times10^7$ in./cycle/psi^{K_4}, and $K_4=1.23$ [8].

Table 2 Elastic properties of SBGA package components and solder

Material	Young's modulus (E) (GPa)	Poisson's ratio (ν)	Coeff. of thermal exp. (α) (/°C)
Solder	24.83	0.4	21×10^{-6}
Copper heatspreader	121	0.38	16.3×10^{-6}
Copper ring	121	0.38	16.3×10^{-6}
Die chip	131	0.3	4.1×10^{-6}
Encapsulant	13.5	0.35	19×10^{-6}
Substrate (BT)	—[a]	—[a]	—[a]
Bonding material	13.5	0.35	19×10^{-6}

[a]Same as PCB (see Table 4).

Table 3 Elastic properties of FR4 material[a]

Properties	Temperature (°C) −55	30	95	125
E_x, GPa	22.4	22.4	20.7	19.3
E_y, GPa	22.4	22.4	20.7	19.3
E_z, GPa	1.6	1.6	1.2	1.0
ν_{xy}	0.02	0.02	0.02	0.02
ν_{yz}	0.143	0.143	0.143	0.143
ν_{zx}	0.143	0.143	0.143	0.143
G_{xy}, GPa	0.63	0.63	0.6	0.5
G_{yz}, GPa	0.199	0.199	0.189	0.167
G_{zx}, GPa	0.199	0.199	0.189	0.167
α_x, /C	15.85×10^{-6}	15.85×10^{-6}	15.85×10^{-6}	15.85×10^{-6}
α_y, /C	19.14×10^{-6}	19.14×10^{-6}	19.14×10^{-6}	19.14×10^{-6}
α_z, /C	80.46×10^{-6}	80.46×10^{-6}	80.46×10^{-6}	80.46×10^{-6}

[a]E, ν, and G denote elastic modulus, Poisson's ratio, and shear modulus, respectively. The subscripts indicate components (see Fig. 1) for orthotropic properties.

Table 4 Elastic properties of BT material[a]

Properties	Temperature (°C) −55	30	95	125
E_x, GPa	24.5	23.13	22.08	21.6
E_y, GPa	24.5	23.13	22.08	21.6
E_z, GPa	1.75	1.65	1.58	1.54
ν_{xy}	0.0273	0.0273	0.0273	0.0273
ν_{yz}	0.195	0.195	0.195	0.195
ν_{zx}	0.195	0.195	0.195	0.195
G_{xy}, GPa	0.689	0.622	0.571	0.547
G_{yz}, GPa	0.218	0.201	0.188	0.183
G_{zx}, GPa	0.218	0.201	0.188	0.183
α_x, /C	13×10^{-6}	13×10^{-6}	13×10^{-6}	13×10^{-6}
α_y, /C	15×10^{-6}	15×10^{-6}	15×10^{-6}	15×10^{-6}
α_z, /C	60×10^{-6}	60×10^{-6}	60×10^{-6}	60×10^{-6}

[a]E, ν, and G denote elastic modulus, Poisson's ratio, and shear modulus, respectively. The subscripts indicate components (see Fig. 1) for orthotropic properties.

4 Equivalent Global Model

Figures 7(*a*) and 7(*b*) display global models (quarter) of fpBGA and SBGA packages, respectively. The associated finite element discretizations by ABAQUS (Version 6.5) [20] involve 8- and 20-noded solid elements, respectively. For the fpBGA package, all solder joints were replaced by an equivalent two-parameter diamond model. However, for the SBGA package, all solder joints except the critical solder joint, which is located at the farthest corner from the center, were replaced by an equivalent eight-parameter general model. In both cases, Option 2 was invoked in solving the proposed optimization problem, leading to optimal values of equivalent sizes. Figures 8(*a*) and 8(*b*) show comparisons of reaction force histories (all three components) from the equivalent diamond model (R_e) and the actual solder joint (R_a), both of which were calculated at optimal size parameters. Clearly, the reaction forces are close to each other, supporting the accuracy of the proposed equivalent model. In contrast, Fig. 8(*c*), which depicts the reaction force history from a volume-averaged equivalent brick model, produces grossly inaccurate results when com-

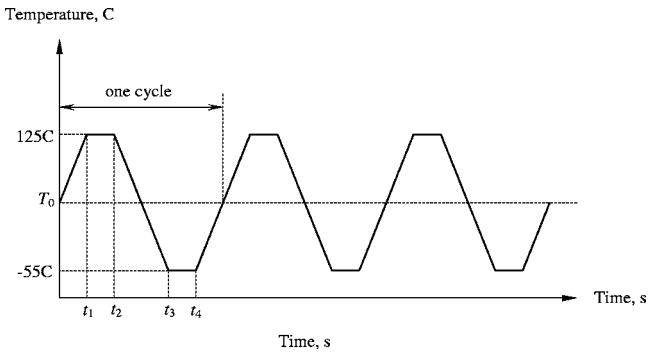

Fig. 6 Thermal load cycles

Table 5 Parameters of prescribed temperature history

Parameters	Package fpBGA	SBGA
T_0 (C)	30	25
t_1 (s)	700	720
t_2 (s)	1700	2000
t_3 (s)	2900	3100
t_4 (s)	4300	3900

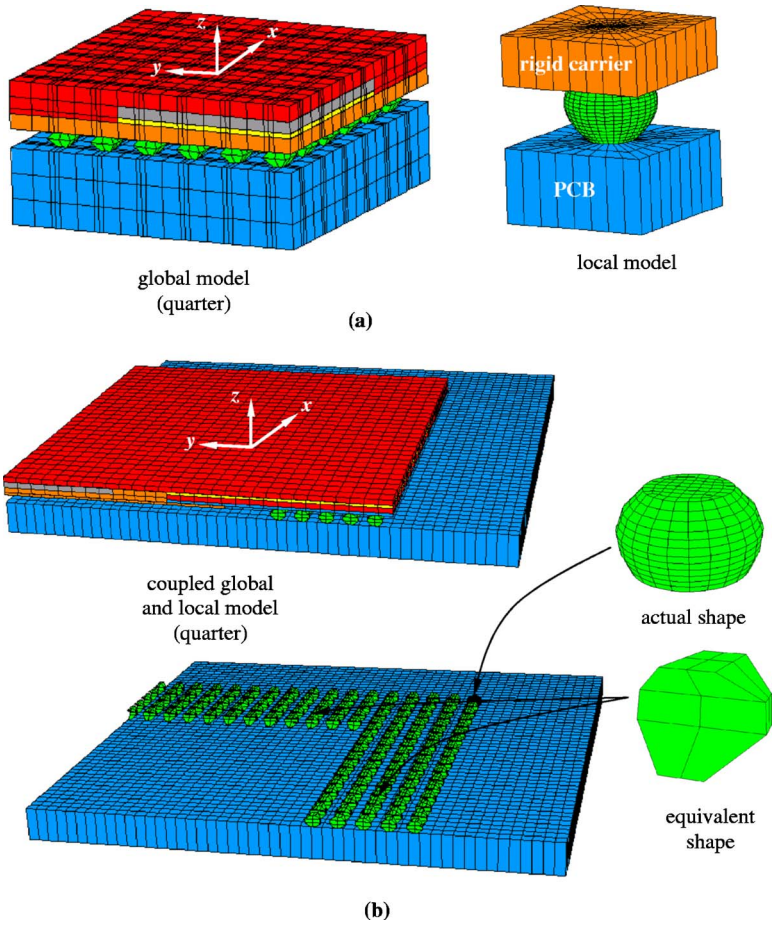

Fig. 7 Global and local models: (*a*) fpBGA; and (*b*) SBGA

pared with those in Fig. 8(*b*). A similar comparison of reaction force histories is presented in Fig. 9 for the SBGA package, which again delineates the deficiency of the volume-averaging technique for equivalent models. It is worth noting that due to a relatively complicated design of the SBGA package, an equivalent general model involving eight parameters, as shown in Fig. 2(*c*), was required to reach an optimal solution. Therefore, existing models that are based on equivalent beams or bricks are unable to simulate global behavior accurately.

In generating the global model of the SBGA package, Fig. 7(*b*), shows the equivalent shape for noncritical solder joints and the actual shape for the critical solder joint. By doing so, the global and local analyses are coupled together without requiring submodeling. Although more efficient than the two-step sequential analyses, a practical dilemma of the coupled approach is to match the fine mesh associated with the critical solder joint with the coarse mesh elsewhere. In this work, the mesh matching requirement was sidestepped by appropriately constraining deformation at common surfaces of fine and coarse meshes, and was achieved by invoking the "tie" option in ABAQUS. However, higher-order elements, such as 20-noded quadratic solid elements, were required and employed for the "tie" option to generate accurate results. The Appendix describes a simple test problem and associated numerical results for a limited verification of the tie option.

5 Experimental Validation of Deformation

Selective experimental works were undertaken for evaluating the global–local methodology. The tests involved measuring in-plane displacements of the fpBGA package over a temperature range using the high accuracy strain mapping (HASMAP) technique. In addition, out-of-plane displacements of both the fpBGA package and package–board assembly were determined by the Moiré interferometry measurement.

5.1 fpBGA Package Only. The FEA and HASMAP measurements of the package with removed solder balls were performed to determine in-plane displacements when the package temperature is raised from 35°C to 125°C. Points *A*, *B*, *C*, and *D* in Fig. 10(*a*) define the quarter of the package analyzed. Figures 10(*b*) and 10(*c*) compare predicted FEA results with measured *x* displacements of the package (quarter), in which the experimental values are linearly fitted to eliminate noisy data. The agreement between FEA and HASMAP results is excellent. In addition, the predicted maximum *x* displacement of 8.1 μm satisfactorily correlates with the experimental value of 7.6 μm. A similar trend is expected for *y* displacements of the package and hence is not presented in this paper for brevity.

Figure 11 displays various fringes from the Shadow Moiré testing of the package at −21°C, −3°C, 10°C, 21°C, 35°C, 90°C, 125°C, and 160°C. The relative out-of-plane displacement, defined as the difference between *z* displacements at the center and at a corner on the solder (stripped) side of the package, was both calculated (FEA) and measured (Shadow Moiré) with lower and upper bounds and is plotted against the temperature in Fig. 12. The simulation result matches the experimental trend well.

5.2 fpBGA Package and Board Assembly. Figure 13(*a*) shows a setup of determining out-of-plane displacements of solder balls (shaded area) in the package–board assembly by the global FEA model of Fig. 7(*a*) and Shadow Moiré measurements. The relative out-of-plane displacement of a solder ball in the shaded

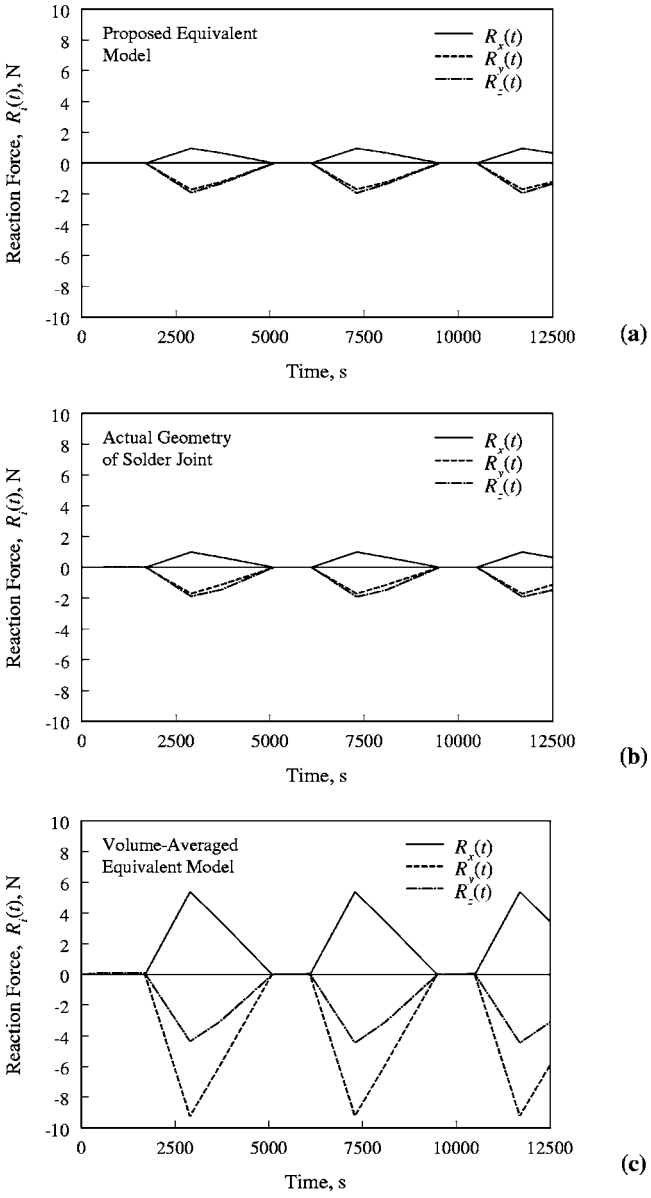

Fig. 8 Reaction force histories for fpBGA: (*a*) proposed equivalent model; (*b*) actual solder joint; and (*c*) volume-averaged equivalent model

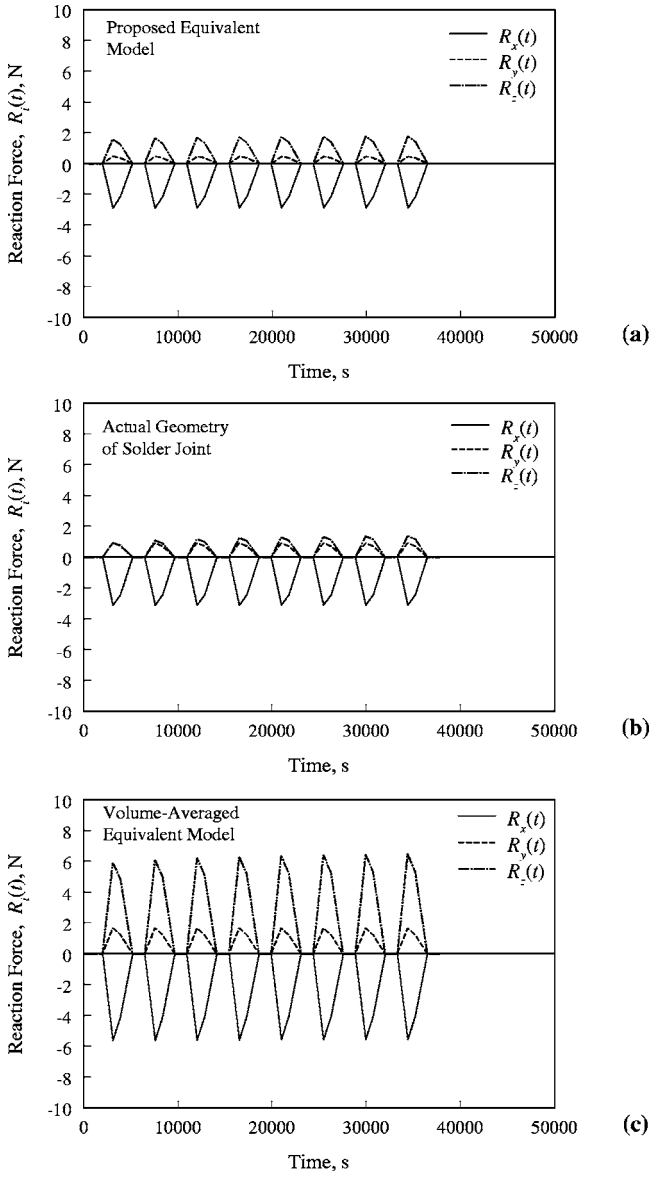

Fig. 9 Reaction force histories for SBGA: (*a*) proposed equivalent model; (*b*) actual solder joint; and (*c*) volume-averaged equivalent model

area, defined as the difference between z displacements at the top and at the bottom of that solder ball, was calculated and is plotted in Fig. 13(*b*). The applied temperature linearly varies from 35°C to 125°C with a ramp rate of 1.5°C/s and a hold time of 1000 s. From the FEA result in Fig. 13(*b*), a solder-ball compression (−4.4 μm) is predicted at the center, while in the middle of the edge (2.56 μm) and at the corner (6.72 μm), the solder balls experience tension. The corresponding Shadow Moiré values of relative out-of-plane displacement in the middle of the edge and at the corner are 5.6 μm and 7.15 μm, respectively, and are also plotted in Fig. 13(*b*). Although FEA significantly underpredicts the relative displacement of the solder ball in the middle of the edge, there is a good agreement between simulation and experimental results for the corner solder ball, which is typically the critical solder joint that determines package durability.

6 Fatigue Life Analysis

Figures 14(*a*) and 14(*b*) show contour plots of predicted fatigue crack-initiation lives (N_i) of the fpBGA and SBGA packages, respectively, obtained by using the strain-based Coffin–Manson equation (Eq. (3)). The local stresses and strains were calculated by the proposed global–local methodology. The predicted minimum (strain-based) crack-initiation lives, which occur at the critical point of the interface between solder joint and substrate or PCB, are only 144 and 204 cycles for the fpBGA and SBGA packages, respectively. However, the corresponding crack-initiation lives of both packages using the cyclic inelastic strain energy density at the critical point (Eq. (4)), also obtained from the global–local methodology, are 460 and 2343 cycles, respectively. In both strain- and energy-based predictions, the initiation lives and the associated values of the strain amplitude ($\Delta\epsilon/2$), the cyclic energy density (ΔW), and the final crack length (a_c) are listed in Table 6. The predicted initiation lives based on the strain are 3–11 times smaller than those based on the strain energy density. The difference in strain- and energy-based predictions of crack-initiation lives are due to different damage parameters in Eqs. (3) and (4). The fatigue durability testing by the daisy chain technology, also carried out in this work, suggests that both packages should survive at least 2500 thermal cycles (test terminated

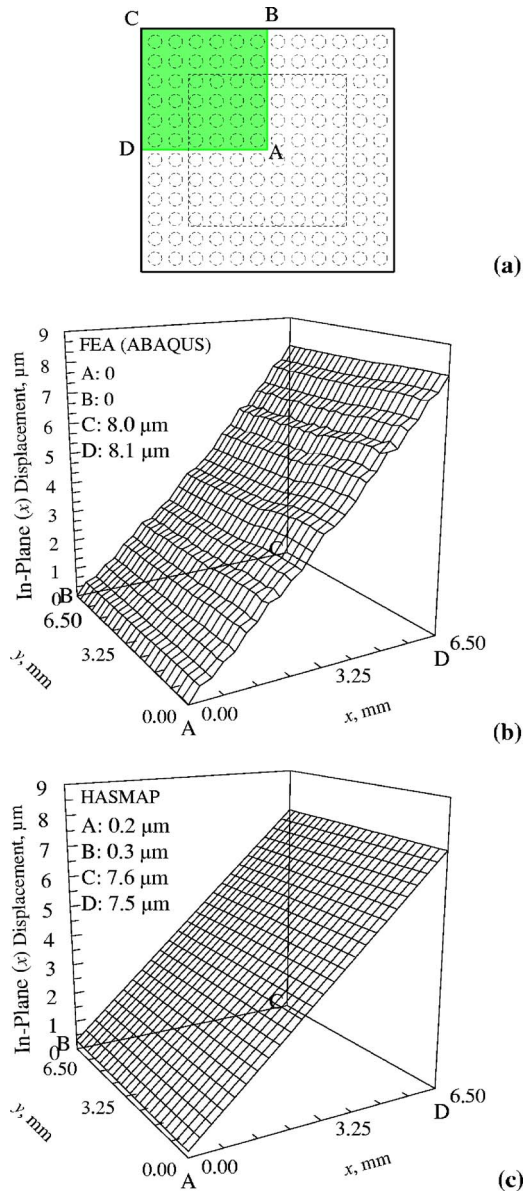

Fig. 10 In-plane *x* displacement of fpBGA package: (*a*) setup; (*b*) simulation; and (*c*) experiment (fitted)

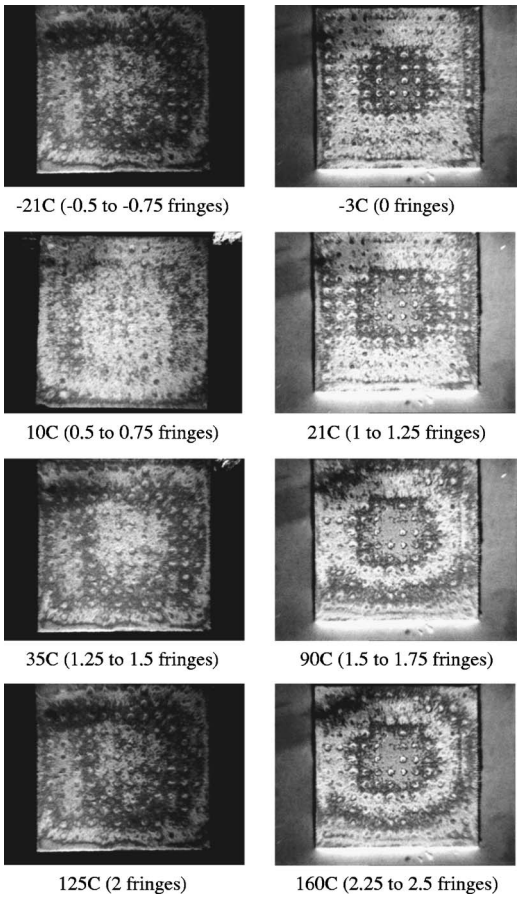

Fig. 11 Out-of-plane displacement of fpBGA package (1 fringe=9.24 μm)

at 2500 cycles). Therefore, energy-based predictions of crack-initiation lives are closer to the experimental data. Nevertheless, the initiation life only provides a lower-bound estimate of the total fatigue life. This is consistent with recent findings of Lau et al. [7], who demonstrated that 63Sn–37Pb solder material can be quite ductile and tolerates a significant amount of crack propagation before failure. Therefore, for a more realistic prediction, remaining life due to crack propagation must be included.

For crack-propagation analysis, the energy-based method described by Eq. (7) was employed, assuming that the initial (a_0) and final (a_c) crack lengths, respectively, are equal to zero and the solder ball diameter at the critical location. The predicted crack-propagation lives (N_p) are 2045 and 12,805 cycles (see Table 6) for the fpBGA and SBGA packages, respectively, and are 4.5–5.5 times larger than the corresponding crack-initiation lives. Therefore, the total fatigue lives from the energy-based method are 2505 and 15,148 cycles, respectively, both of which exceeded the runout experimental data of 2500 cycles. For the SBGA package, a high-powered optical microcross-sectional examination revealed onset of cracking at the end of testing (i.e., at the end of 2500 cycles). Hence, the relatively large crack-initiation life of the SBGA package predicted using the energy-based method appears reasonable. However, the energy-based method also predicted a very high crack-propagation life for the SBGA package because of lower strain energy density (36% of that in the fpBGA package; see Table 7) and larger critical crack length (180% of that in the fpBGA package; see Table 7). Therefore, further studies are needed for crack-propagation analysis. Based on proposed modeling and simulation results, the SBGA package is more durable than the fpBGA package. The result is expected because the SBGA package has larger solder-ball diameters of upper and lower cross sections than the fpBGA package. Hence, the conclu-

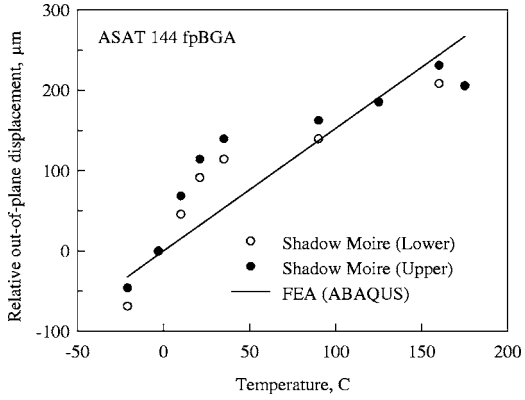

Fig. 12 Relative out-of-plane displacement of fpBGA package

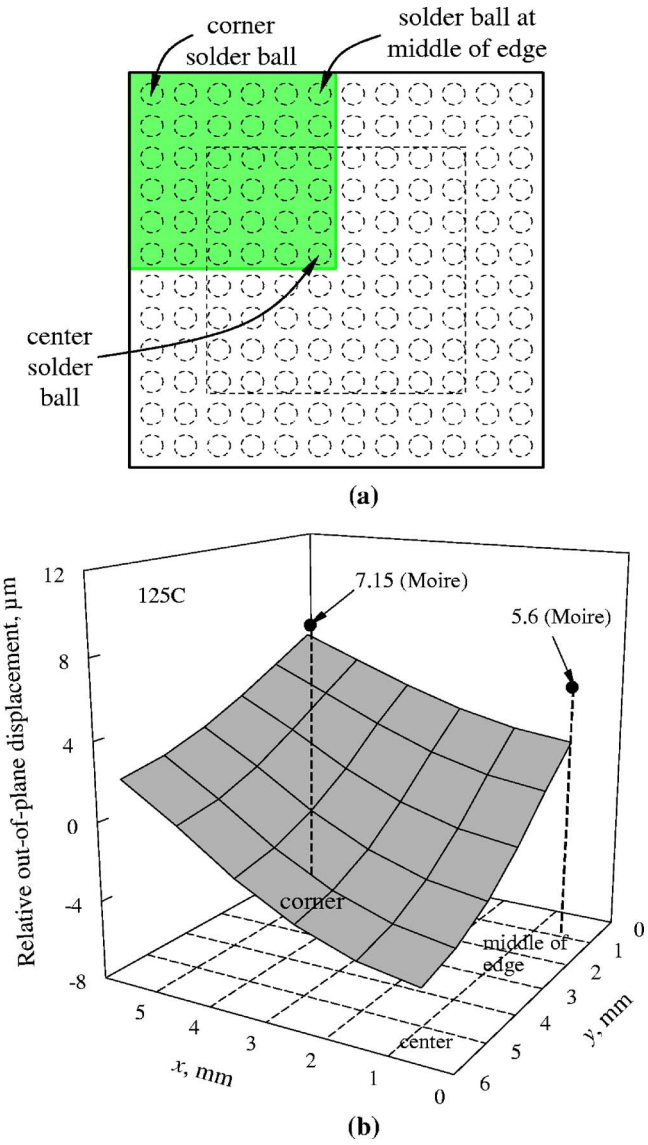

Fig. 13 Out-of-plane displacement of fpBGA package–PCB assembly: (*a*) setup; and (*b*) relative displacement

sion on durability performance is limited to specific designs of packages studied and should not be interpreted as the general trend.

7 Summary and Conclusion

A global–local methodology was developed for predicting mechanical deformation and fatigue durability of solder joints in electronic packaging systems subject to cyclic thermal loading. It involves a global deformation analysis, a local critical solder–joint analysis, and a fatigue life analysis. The methodology was applied to fpBGA and super BGA packages. The global deformation analysis entails a new optimization formulation for determining equivalent models from nonlinear response characteristics of actual solder joints. The simulation results indicate that the volume-averaging technique may be grossly inaccurate. Indeed, a complicated shape of the equivalent model may be required for packages with a complex design (super BGA). Selective experimental efforts were also undertaken to evaluate the predicted deformation characteristics of the fpBGA package. New experimental data were developed for in-plane and/or out-of-plane displacements of the package and the package–board assembly using HASMAP and Shadow Moiré interferometry. In general, a good agreement

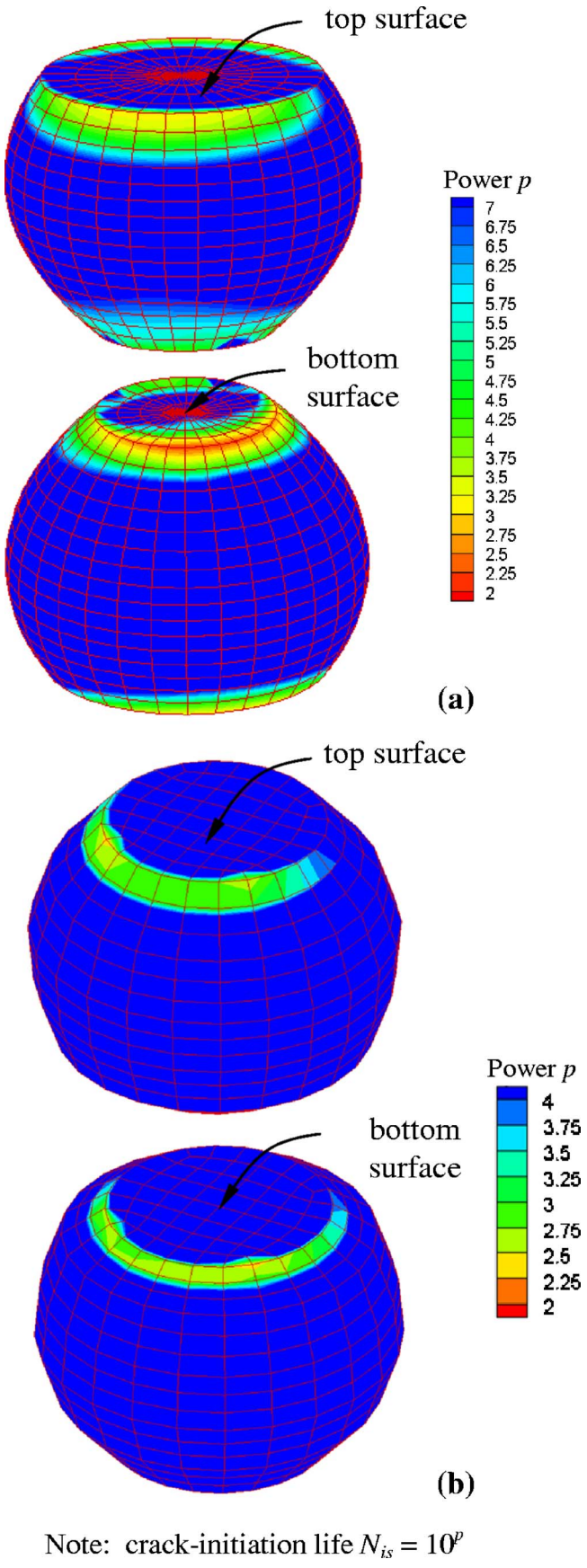

Fig. 14 Contour plots of predicted crack-initiation life: (*a*) fpBGA; and (*b*) SBGA

Table 6 Predicted fatigue lives of fpBGA and SBGA packages[a]

Damage parameters, crack length, and fatigue lives	Package	
	fpBGA	SBGA
$\Delta\epsilon/2$	0.0215	0.0188
ΔW [psi (MPa)]	25.41 (0.1752)	9.25 (0.0638)
a_c [in. (mm)]	0.0118 (0.3)	0.0213 (0.542)
N_{is}, cycles	144	204
N_{ie}, cycles	460	2343
N_{pe}, cycles	2045	12,805
N, cycles	2505	15,148

[a]$\Delta\epsilon/2$=equivalent strain amplitude; ΔW=cyclic inelastic strain energy density; a_c=final crack length; N_{is}=crack-initiation life by strain-based method; N_{ie}=crack-initiation life by energy-based method; N_{pe}=crack-propagation life by energy-based method; and $N=N_i+N_p$=total fatigue life by energy-based method.

was obtained between the simulated results of the proposed methodology and experimental observations of deformations for the fpBGA package studied.

For the durability analysis, the strain-based method significantly underpredicted crack-initiation lives of both packages. On the other hand, the energy-based method provided realistic estimates of crack-initiation lives. The total life predicted using the energy-based method is larger than 2500 cycles—a trend observed experimentally for both packages entailing widely different designs. Based on proposed modeling and simulation results and specific designs of packages studied, the SBGA package is more durable than the fpBGA package.

8 Future Work

The energy-based crack-propagation analysis employing crack length as a damage parameter significantly overpredicted the fatigue life of the SBGA package. Future works include crack-propagation analysis employing the solder-ball cracked area as a damage parameter and correlating the evolution of cracked area with respect to number of thermal cycles with experimental measurements.

Acknowledgment

Work conducted under this study was sponsored by Rockwell Collins, Inc. The authors would like to acknowledge the experimental assistance of Dr. Lisa Fischer, Rockwell Scientific Company, Thousands Oaks, CA.

Appendix

Consider a simple test problem, where two linear–elastic and isotropic solids – a 6 mm×6 mm×1 mm lower solid and a 3 mm×3 mm×3 mm upper solid are perfectly bonded, as shown in Fig. 15(*a*). The Young's modulus and Poisson's ratio of both solids are 200 MPa and 0.3, respectively. The upper solid is subjected to a uniformly distributed load, applied in the x direction with a resultant force of 10 N in the y-z plane. The bottom surface of the lower solid is fixed. Two FEA models with 20-noded brick elements, one involving a traditional compatible mesh without the tie option (Fig. 15(*b*)) and the other involving an incompatible mesh with the tie option (Fig. 15(*c*)), were developed. A linear–elastic analysis was performed.

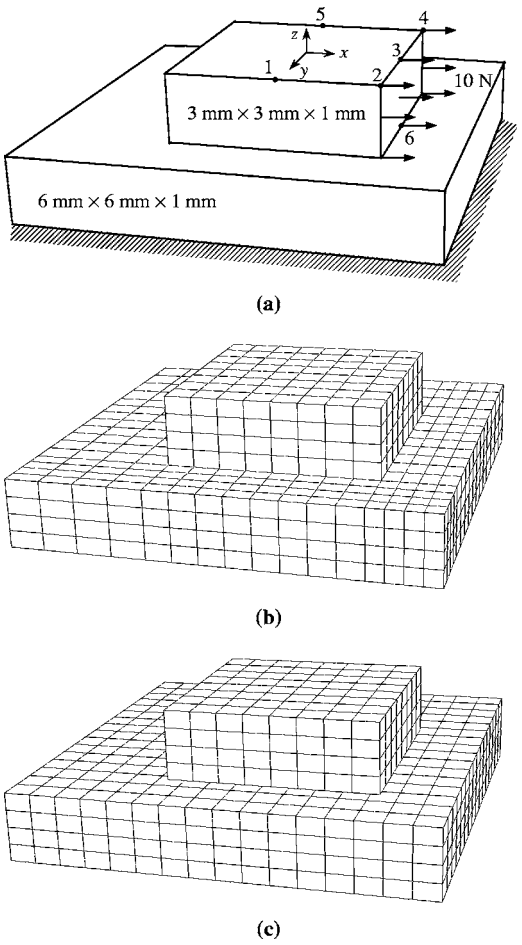

Fig. 15 Verification of the tie option: (*a*) simple test problem; (*b*) compatible mesh without tie option; and (*c*) incompatible mesh with tie option

Displacement components u_x, u_y, and u_z at six key nodes, marked as 1, 2, 3, 4, 5, and 6 in Fig. 15(*a*), were evaluated by both FEA models. The model results, listed in Table 7, indicate that an incompatible mesh employing higher-order elements (20-noded

Table 7 Displacements of the simple test problem

Node	Displacements (mm)[a]					
	Compatible mesh (without tie)			Incompatible mesh (with tie)		
	u_x	u_y	u_z	u_x	u_y	u_z
1	5.382×10^{-2}	9.933×10^{-3}	6.879×10^{-4}	5.325×10^{-2}	9.837×10^{-3}	6.898×10^{-4}
2	1.183×10^{-1}	1.954×10^{-2}	-3.531×10^{-2}	1.173×10^{-1}	1.943×10^{-2}	-3.447×10^{-2}
3	1.174×10^{-1}	-1.6×10^{-4}	-4.243×10^{-2}	1.164×10^{-1}	-1.014×10^{-4}	-4.149×10^{-2}
4	1.185×10^{-1}	-1.986×10^{-2}	-3.515×10^{-2}	1.173×10^{-1}	-1.961×10^{-2}	-3.433×10^{-2}
5	5.397×10^{-2}	-1.024×10^{-2}	7.265×10^{-4}	5.326×10^{-2}	-1.009×10^{-2}	6.643×10^{-4}
6	3.843×10^{-2}	-2.856×10^{-5}	-1.907×10^{-2}	3.693×10^{-2}	-6.787×10^{-6}	-1.624×10^{-2}

[a]u_x, u_y, and u_z are displacements in x, y, and z directions.

brick) and the tie option yields accurate displacement responses when compared with those obtained from a traditional compatible mesh. A subsequent parametric study by varying sizes of the two solids, mesh density, and boundary conditions was also performed, the results of which support the same conclusion. For brevity, the details of the parametric study are not presented in this paper.

References

[1] Mukai, M., Kawakami, T., Takahashi, K., Kishimoto, K., and Shibuya, T., 1998, "Thermal Fatigue Life of Solder Bumps in BGA," JSME Int. J., Ser. A, **41**(2), pp. 260–266.

[2] Cheng, H. C., Chiang, K. N., and Lee, M. H., 1998, "An Effective Approach for Three-Dimensional Finite Element Analysis of Ball Grid Array Typed Packages," ASME J. Electron. Packag., **120**, pp. 129–134.

[3] Yuan, C., and Chiang, K., 2003, "Micro to Macro Thermo-Mechanical Simulation of Wafer Level Packaging," ASME J. Electron. Packag., **125**, pp. 576–581.

[4] Chan, Y., Ju, T., Hareb, S., Lee, Y., Wu, J., and Lii, M., 2002, "Reliability Modeling for Ball Grid Array Assembly with a Large Number of Warpage Affected Solder Joints," ASME J. Electron. Packag., **124**, pp. 246–253.

[5] Wang, T. H., and Lai, Y. S., 2005, "Submodeling Analysis for Path-Dependent Thermomechanical Problems," ASME J. Electron. Packag., **127**, pp. 135–140.

[6] Lau, J. H., 1991, *Solder Joint Reliability*, Van Nostrand Reinhold, New York.

[7] Lau, J. H., Pan, S. H., and Chang, C., 2002, "A New Thermal-Fatigue Life Prediction Model for Wafer Level Chip Scale Package (WLCSP) Solder Joints," ASME J. Electron. Packag., **124**, pp. 212–220.

[8] Darveaux, R., 2002, "Effect of Simulation Methodology on Solder Joint Crack Growth Correlation and Fatigue Life Prediction," ASME J. Electron. Packag., **124**, pp. 147–154.

[9] Engelmaier, W., 1983, "Fatigue Life of Leadless Chip Carrier Solder Joint During Power Cycling," IEEE Trans. Compon., Hybrids, Manuf. Technol., **6**(3), pp. 234–235.

[10] Solomon, H. D., 1989, "Strain-Life Behavior in 60/40 Solder," ASME J. Electron. Packag., **111**, pp. 75–82.

[11] Dasgupta, A., Oyan, C., Barker, D., and Pecht, M., 1992, "Solder Creep-Fatigue Analysis by an Energy Partitioning Approach," ASME J. Electron. Packag., **114**, pp. 152–160.

[12] Akay, H., Liu, Y., and Rassaian, M., 2003, "Simplification of Finite Element Models for Thermal Fatigue Life Prediction of PBGA Packages," ASME J. Electron. Packag., **125**, pp. 347–353.

[13] Zhang, T., Choi, K. K., Rahman, S., Cho, K., Perry, B., Shakil, M., and Heitkamp, D., 2006, "A Response Surface and Pattern Search Based Hybrid Optimization Method and Application to Microelectronics," Struct. Multidiscip. Optim., **32**(4), pp. 327–345.

[14] Dowling, N. E., 1999, *Mechanical Behavior of Materials: Engineering Methods of Deformation, Fracture, and Fatigue*, 2nd ed., Prentice–Hall, Englewood Cliffs, NJ.

[15] Guven, I., Kradinov, V., Tor, J., and Madenci, E., 2004, "Strain Energy Density Criterion for Reliability Life Prediction of Solder Joints in Electronic Packaging," ASME J. Electron. Packag., **126**, pp. 398–405.

[16] Lau, J., Lee, S., and Chang, C., 2000, "Solder Joint Reliability of Wafer Level Chip Scale Packages (WLCSP): A Time-Temperature-Dependent Creep Analysis," ASME J. Electron. Packag., **122**, pp. 311–316.

[17] Wiese, S., and Meusel, E., 2003, "Characterization of Lead-Free Solders in Flip Chip Joints," ASME J. Electron. Packag., **125**, pp. 531–538.

[18] Limaye, P., Vandevelde, B., Vandepitte, D., and Verlinden, B., 2005, "Crack-Growth Rate Measurement and Analysis for WLCSP Sn-Ag-Cu Solder Joints," *Proceedings of SMTA International Conference*, Chicago, IL, September.

[19] Rahman, S., Choi, K. K., and Zhang, T., 2005, "Input Data for fpBGA and SBGA Packages," Rockwell Collins, Iowa City, IA, Interim Report.

[20] ABAQUS, 2005, User's Guide and Theoretical Manual, Version 6.5, Hibbitt, Karlsson, and Sorenson, Inc., Pawtucket, RI.